Spectroscopy of an ultracold Rydberg gas and signatures of Rydberg–Rydberg interactions

INSTITUTE OF PHYSICS PUBLISHING JOURNAL OF PHYSICS B: ATOMIC, MOLECULAR AND OPTICAL PHYSICS

J. Phys. B: At. Mol. Opt. Phys. **38** (2005) S321–S332 doi:10.1088/0953-4075/38/2/023

Spectroscopy of an ultracold Rydberg gas and signatures of Rydberg–Rydberg interactions

Kilian Singer, Markus Reetz-Lamour, Thomas Amthor, Simon Fölling[1], Michaela Tscherneck[2] and Matthias Weidemüller

Physikalisches Institut der Albert-Ludwigs-Universität Freiburg, Hermann-Herder-Str. 3, 79104 Freiburg, Germany

E-mail: kilian.singer@physik.uni-freiburg.de and m.weidemueller@physik.uni-freiburg.de

Received 6 August 2004, in final form 29 September 2004
Published 5 January 2005
Online at stacks.iop.org/JPhysB/38/S321

Abstract

We report on experiments on Rydberg–Rydberg interaction-induced effects in a gas of ^{87}Rb Rydberg atoms. A compact setup for two-photon continuous-wave excitation of high-lying Rydberg states out of an ultracold atomic gas is presented. The performance of the apparatus is characterized by high-resolution spectroscopy of Rydberg states. Signatures of interaction-induced effects are identified by qualitatively analysing the dependence of Rydberg excitation spectra on the intensity and the duration of the second-step laser excitation.

1. Introduction

Rydberg atoms have been extensively studied over many decades [1]. With the advent of trapping and cooling techniques it has become possible to excite Rydberg atoms out of an ultracold ($T < 1$ mK) atomic gas ('frozen Rydberg gas' [2, 3]). In contrast to atom beam experiments, Rydberg atoms in a frozen Rydberg gas do not move significantly over the experimental time scales given by the Rydberg atom lifetime. As the atom–atom interaction increases strongly with the principal quantum number n, frozen Rydberg gases offer unique possibilities for the study of few-body and many-body interactions, since even weak interactions induce measurable effects. Exotic molecules bound by ultralong-range interactions have been proposed in theory [4, 5] but have not yet been found experimentally. Signatures of Rydberg–Rydberg interactions in a frozen Rydberg gas have recently been observed as diffusion of excitation [2, 3], Rydberg-state changing collisions [6], molecular crossover resonances [7] and as the onset of a van der Waals blockade [8, 9]. The latter

[1] Present address: Quantum, Johannes-Gutenberg-Universität Mainz, 55128 Mainz, Germany.
[2] Present address: Department of Physics and Astronomy, University of Rochester, Rochester, NY 14627-0171, USA.

effect can be exploited to perform quantum information processing with Rydberg atoms [10, 11].

In this paper we present experiments employing narrow-bandwidth continuous-wave (cw) excitation to produce a frozen Rydberg gas from ^{87}Rb atoms trapped in a magneto-optical trap. We describe in detail our compact experimental setup for resonant two-photon excitation into high-lying Rydberg states out of an ultracold Rydberg gas. As a particular feature of the apparatus, we have implemented Raman-sideband cooling which results in temperatures in the sub-μK range. In a spectroscopic approach, Rydberg–Rydberg interactions are studied by analysing excitation spectra as a function of density, excitation rate, excitation time and interaction strength (as a function of principal quantum number n). The density dependence of excitation which is extensively discussed in [9] provides evidence for a suppression of Rydberg excitation through long-range interactions between the Rydberg atoms. In this paper we show additional measurements complementing the data presented in [9] and providing additional experimental material for an understanding of the dynamics of interacting Rydberg gases. The paper is structured as follows: in section 2 we describe our experimental approach to a frozen Rydberg gas. Spectra for the characterization and calibration of our experiment are shown in section 3. Section 4 presents spectroscopic signatures of Rydberg–Rydberg interactions. The results are discussed in section 5.

2. Preparation of an ultracold Rydberg gas

2.1. Vacuum system

The experimental setup is schematically shown in figure 1(a). A cloud of cold ^{87}Rb atoms is prepared in a magneto-optical trap (MOT) [12]. The magnetic coils needed for the MOT are placed inside a stainless steel cube of side length 124 mm (Kimball Physics) providing optical access along the three mutually orthogonal main axes and along the four diagonals. The six main windows are used for the trapping and cooling laser beams, while two diagonals serve for electrical feedthroughs. The Rydberg excitation laser beam passes through another diagonal, and the fourth diagonal is used for fluorescence monitoring. The atom cloud is loaded from rubidium vapour released from a dispenser (SAES Getters) situated close to the centre of the vacuum cube, which is evacuated to a base pressure below 10^{-10} mbar.

In order to apply well-defined electric fields for Rydberg atom manipulation and ionization, the MOT is placed between two metal grids spaced 13.2 mm apart with an optical transmission of 95% through which the MOT laser beams pass almost undisturbed. Rydberg atoms are detected by field ionization. Ions and electrons are accelerated by electric fields onto oppositely placed micro-channel plates (MCP) which amplify the charge signal. Calibration of the MCP signals is described in section 2.4.

2.2. Laser system and magneto-optical trap

The laser beams used for the MOT are emitted by a novel laser system which coherently adds two laser beams [13] as shown in figure 1(b). An external cavity diode laser (ECDL) electronically locked to an atomic transition with a Doppler-free dichroism spectroscopy [14] serves as the primary frequency reference. The laser beam is frequency-shifted with an acousto-optical modulator (AOM) to a detuning of 1.5Γ (natural linewidth $\Gamma/2\pi = 6.1$ MHz) below the transition $5S_{1/2}(F = 2) \rightarrow 5P_{3/2}(F = 3)$ (see figure 2) for atom cooling and trapping in the MOT. The beam seeds two laser diodes which are coherently added to produce a single laser beam with an intensity which is equal to the sum of the intensities of the two

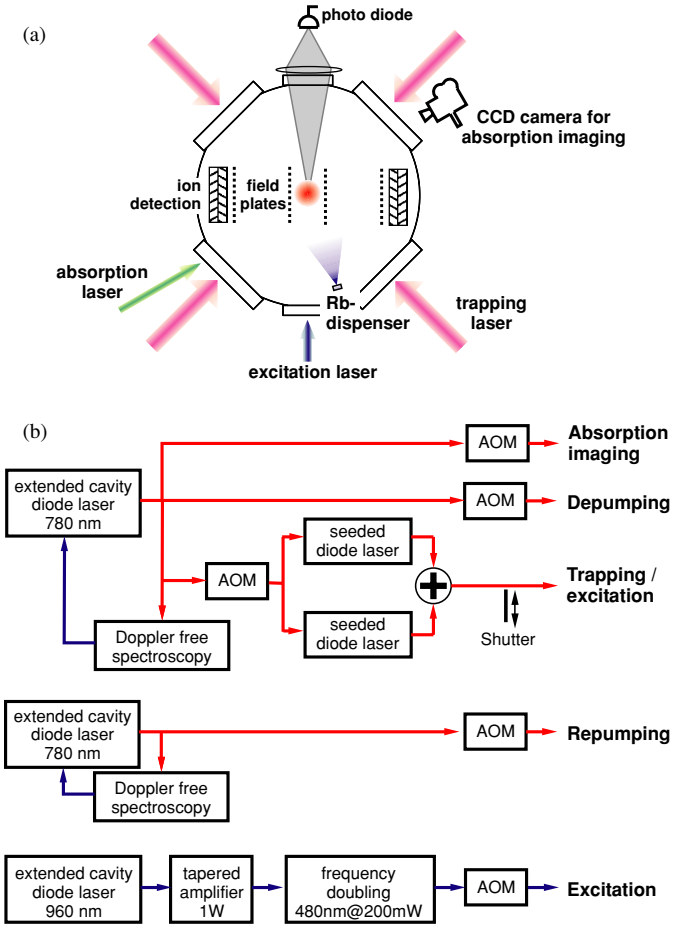

Figure 1. (a) Schematic of the experiment. (b) Schematic of the laser system for cooling, trapping and Rydberg excitation. For further details see text.

sources [13]. The resulting beam is guided to the vacuum chamber through a single mode fibre. The addition scheme provides 70 mW laser power at the fibre output. The fibre output beam is split into six beams, which pass quarter-wave plates and are sent through the main windows of the vacuum chamber.

The cooling and trapping beams are superimposed with beams from a second ECDL (see figure 1(b)) driving the transition $5S_{1/2}(F = 1) \rightarrow 5P_{3/2}(F = 2)$ in order to repump atoms that have been off-resonantly excited out of the cooling and trapping cycle (see figure 2). This laser is locked to an atomic transition using Doppler-free frequency-modulation spectroscopy [15]. A small portion of the frequency-reference ECDL is frequency-shifted with an AOM and is used to intentionally depump atoms out of the cooling and trapping cycle. This allows for systematic measurements of density-dependent effects as described in detail in [9]. All laser beams can be switched or attenuated by AOMs in combination with mechanical shutters [16] to allow for controlled manipulation and excitation of internal states.

The frequency-reference ECDL laser also provides a beam for absorption images of the atomic cloud in the MOT which are detected by a CCD camera. Size and density of the cloud are determined by analysing absorption images. Temperature measurements are performed

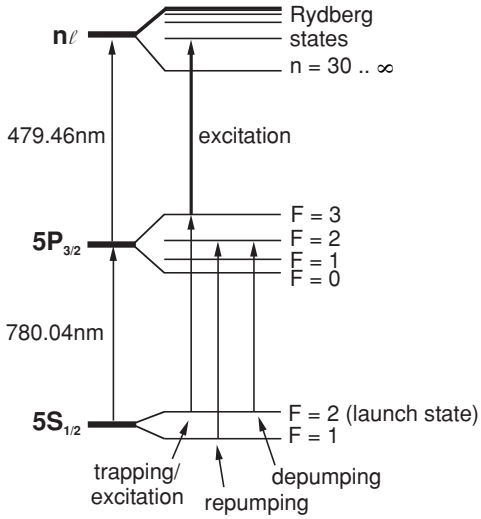

Figure 2. Relevant energy levels of ^{87}Rb for cooling, trapping and Rydberg excitation. The $5S_{1/2}(F = 2)$ state serves as the launch state for two-step Rydberg excitation via the $5P_{3/2}(F = 3)$ state. By depumping atoms into the $5S_{1/2}(F = 1)$ state one can modify the density of atoms in the launch state in a controlled way.

by monitoring the ballistic expansion of the cloud after turning off all trapping lasers. The number of atoms in the MOT is monitored by collecting the fluorescence light on a photodiode. The measured fluorescence signal is calibrated with absorption images to yield absolute atom numbers.

With this setup between 10^7 and 10^8 ^{87}Rb atoms are trapped at a peak density of about 10^{10} cm^{-3} with loading times of roughly 5 s. The steady state temperature of the MOT is of the order of 100 μK. The temperature can be reduced in pulsed operation using optical molasses [17] (down to 4.5 μK) or 3D degenerate Raman sideband cooling (below 1 μK). The latter method has already been successfully implemented by our group [18], but has not been used for the results presented here.

2.3. Excitation and detection

Out of the ultracold atomic gas atoms are prepared in Rydberg states in a two-photon excitation scheme. The first photon is provided by tuning the cooling and trapping laser beam of the MOT into resonance, while the second photon is generated by a commercial system (Toptica TA-SHG 110) consisting of an ECDL at 960 nm which is amplified to 1 W and frequency-doubled to 479 nm with a linewidth <2 MHz. The wavelength of this laser can be tuned by ± 1 nm to address Rydberg levels starting from $n \simeq 30$ up to the ionization threshold (see figure 2).

The blue excitation laser is switched on for a variable time (typically 20 μs) after the MOT laser has been tuned to resonance. The delay between changing the MOT laser detuning and switching the blue laser can be precisely controlled on the 100 ns level. The Rydberg excitation cycle is completed by applying an ionizing field to the central grids and collecting the ions and electrons on the micro-channel plates (MCP) (see figure 1). The overlap region of the excitation laser beam, which has a waist of 80(10) μm, with the MOT of 1.2 mm $1/e$-diameter defines a cylindrical Rydberg excitation volume of 0.011 mm^3.

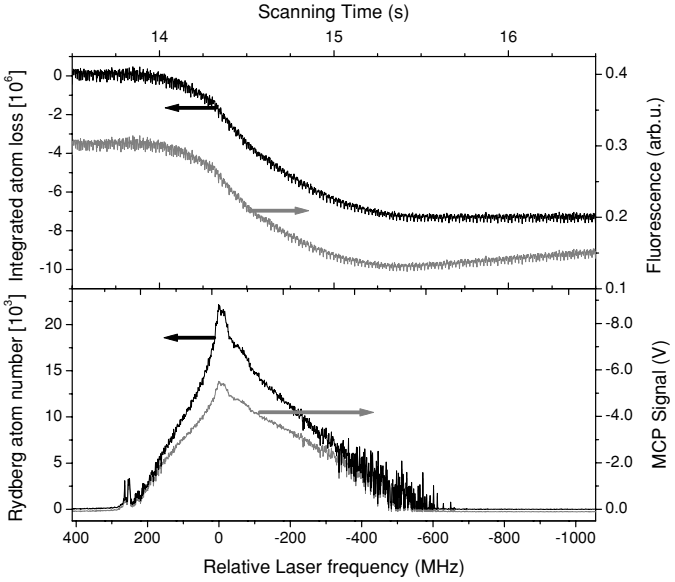

Figure 3. MCP calibration procedure. The blue excitation laser is flashed on for 20 μs with a repetition rate of 500 Hz while being scanned over a Rydberg resonance. The upper graph shows the corresponding fluorescence signal (grey line, right axis) which is calibrated by absorption imaging and corrected for MOT reloading during the scan (black line, left axis). The lower graph depicts the original MCP signal (grey line, right axis) and the signal after correcting saturation effects by integrating and fitting to the atom loss signal (black line, left axis). For details on the calibration procedure see text.

2.4. MCP calibration

To determine the absolute number of Rydberg atoms N_R, the MCP signal is compared to the flourescence loss which in turn is calibrated by absorption images. The atom number determined by absorption imaging has an uncertainty of about a factor of 2 due to systematic errors.

The calibration proceeds as follows: the frequency of the blue excitation laser is slowly scanned over a Rydberg resonance. During the scan both fluorescence and MCP signals are monitored simultaneously as shown in figure 3. The fluorescence signal is corrected for the atoms that are continuously reloaded into the MOT by using the MOT loading rate which is determined in an independent measurement. The corrected fluorescence signal shown as the black curve in the upper graph of figure 3 then gives the accumulated number of atoms lost from the MOT by excitation into the Rydberg state. This curve reflects the integral over the MCP signal. However, for a comparison, the saturation behaviour of the MCP must be taken into account. As we do not have exact knowledge of this behaviour, we compare two different heuristic saturation functions for the MCP signal $U_{\mathrm{MCP}} = \alpha N_R/(1 + N_R/N_{\mathrm{sat}})$ and $U_{\mathrm{MCP}} = \alpha' N_R(1 - \exp(-N_R/N'_{\mathrm{sat}}))$. Using these expressions, the MCP signal is transformed to particle numbers and its integral is fitted to the corrected fluorescence signal. In this way, the parameters α and N_{sat} are determined. We find the resulting corrected MCP signals for the two functions to agree within 10% showing that the exact shape of the saturation function is of minor influence on the calibration procedure. It must be pointed out that this procedure is very sensitive only for strongly saturated MCPs. It is consistent with independent measurements

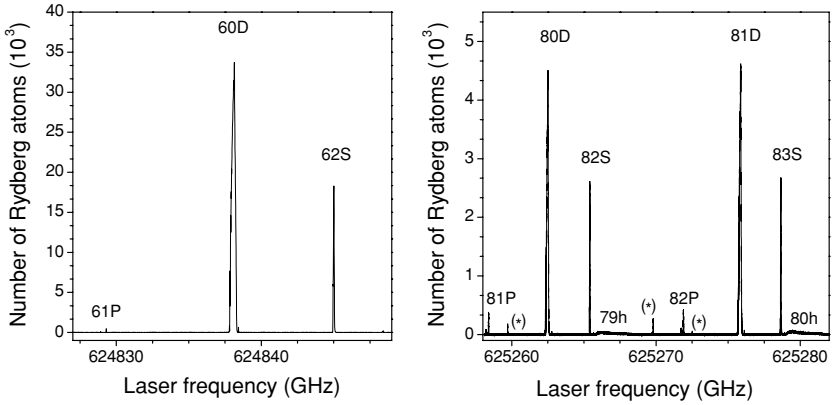

Figure 4. Rydberg spectra at $n \simeq 60$ and $n \simeq 80$. The x-axis is the frequency of the blue excitation laser providing the second step in the two-photon excitation scheme. Besides the dipole-allowed nS and nD states, residual electric fields also allow for the excitation of nP and the hydrogen-like nh ($n\ell$, $\ell \geqslant 3$) states. The lines marked with (*) have not been assigned so far.

of the MCP response at two different bias voltages. However, both methods cannot give a lower bound for the saturation signal of the MCP and therefore lead to a systematic error towards higher Rydberg atom numbers as depicted in figure 7(b). This upper bound is given by assuming a fully saturated MCP at the highest MCP signals observed.

3. High-resolution spectroscopy of Rydberg states

3.1. Assignment of spectra

Figure 4 shows spectra around principal quantum numbers $n = 60$ and $n = 80$. Only excitations of nS and nD states are dipole-allowed in the two-photon excitation scheme employed in our experiments (see figure 2). However, small residual electric fields (<0.2 V cm^{-1}) break the selection rules and therefore allow for the excitation of nP and $n\ell$ states ($\ell \geqslant 3$). The latter states are called hydrogen-like states because of their negligible quantum defect. The residual field is mainly a result of the high voltages at the MCPs and inhomogeneities induced by the highly transmissive grids (see section 2). While field components perpendicular to the grids can be compensated by a small bias field, parallel components cannot be cancelled. These components are determined by Stark map measurements as will be explained in section 3.2. While this field is too weak to excite $\ell \geqslant 3$ states at $n \simeq 60$, hydrogen-like states are excited at $n \simeq 80$ since higher n leads to higher sensitivity to external fields. On the other hand, the excitation rate for the dipole-allowed transitions actually decreases for increasing n [1]. The linewidths of non-saturated transitions at low excitation rates are of the order of 10 MHz mainly determined by the linewidth of the saturated first excitation step. On this level of precision, the influence of the magnetic quadrupole field of the MOT can be neglected.

The absolute frequency of the resonances was measured by a commercial wavemeter (Burleigh) with an accuracy of 500 MHz. The spectral position of all major resonances in the spectrum coincides with the expected values taking into account the corresponding quantum defects of the levels [1]. However, the lines in the $n = 80$ spectrum marked with (*) could not be related to atomic resonances even when taking other hyperfine levels of the $5S_{1/2}$ ground

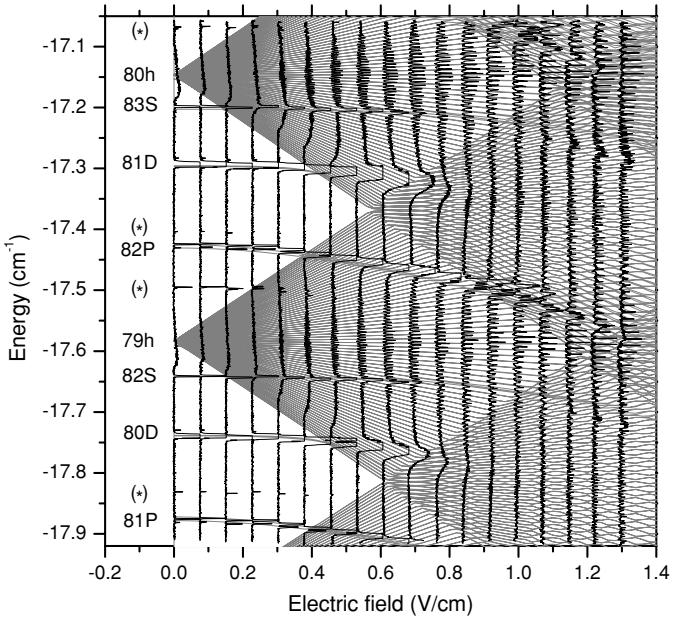

Figure 5. Electric field dependence of the excitation spectra for $n \simeq 80$ (Stark map). The experimental data (black) are overlapped with the result of perturbation theory (shown as grey lines).

and $5P_{3/2}$ intermediate states into account (e.g. off-resonant two-photon excitation from the $5S_{1/2}(F = 1)$ state, a so-called hyperfine ghost, see figure 2). Remarkably, these lines do not appear at $n \simeq 60$ although the excitation rate is higher there. Non-atomic resonances have been found to be caused by two-particle interactions leading to level crossings [7], however this explanation does not seem to be in accordance with our data. The interpretation of these resonances must therefore await further experiments studying the dependence of these lines on density and detuning of the first excitation step. In addition, molecular potential curves are needed in order to relate these resonances to possible level crossings.

3.2. Stark map

As Rydberg states exhibit large polarizabilites, Rydberg excitation spectra depend on static electric fields [19]. The dependence of the spectrum at $n \simeq 80$ is shown in figure 5. The line positions of the observed resonances can be compared to quantum mechanical calculations for Rydberg atoms in electric fields [20] and allow for a calibration of the electric field at the position of the atoms. In particular, the field component perpendicular to the field plates can be precisely compensated in this way.

The excitation rate of dipole-forbidden transitions (as for nP states) scales quadratically with the electric field. By measuring the peak area of the 82P line for varying electric fields, we determined the residual field to be 0.16 V cm^{-1} (component parallel to the grids). An alternative calibration method is to monitor the splitting of the hydrogen-like states which grows linearly with increasing electric field. This provides a similar value of 0.12 V cm^{-1} for the residual field.

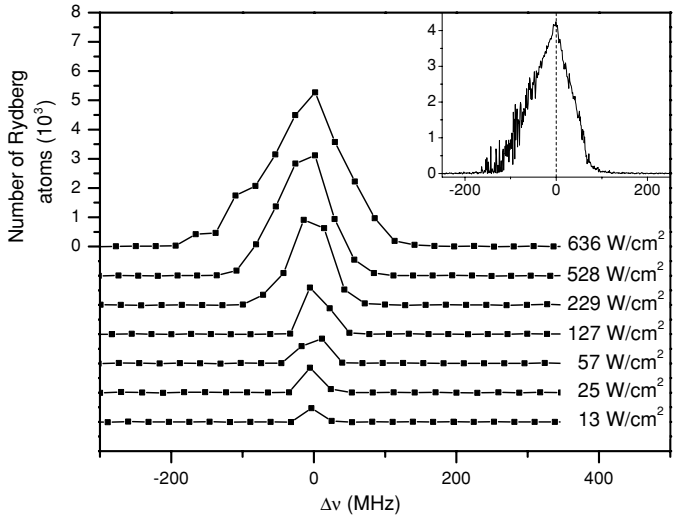

Figure 6. Excitation spectrum of the 82S resonance for different intensities of the blue laser driving the second excitation step in the two-photon excitation scheme (see figure 2). The first excitation step is saturated. The inset shows a high-resolution spectrum of the same transition.

4. Spectroscopic signatures of Rydberg–Rydberg interactions

The first spectroscopic signs of interaction-induced effects in Rydberg gases were seen in atomic beam experiments [21]. In these experiments, atoms at densities of $\simeq 10^{13}$ cm^{-3} were excited into Rydberg states ($n \sim 40$) using broad-bandwidth pulsed lasers. With increasing laser power (and thus increasing Rydberg atom densities) the excitation lines broaden, which was explained by the dipole–dipole interaction in dense Rydberg gases. Figure 6 shows the result of an equivalent measurement, but now performed in the $n \simeq 80$ manifold with a narrow-bandwidth continuous-wave laser excitation. This setup allows for much higher resolution and leads to similar findings at launch state densities that are about three orders of magnitude smaller ($\simeq 10^{10}$ cm^{-3}). With increasing laser intensity the resonance lines broaden significantly. The inset in figure 6 shows a high-resolution scan of the same transition, revealing that the line broadening is asymmetric and that the red wing of the resonance contains some pronounced structure. Additionally, we observe a saturation of the peak height, which we attribute to an excitation inhibition at exact resonance. A shift of the resonance lines could not be seen in our experiment, as we do not have absolute values for the frequency axis. The peaks in figure 6 are all centred around $\Delta\nu = 0$ at their maximum value.

There are several possible explanations that could account for the observed line broadening which are also discussed in [21]. Pure saturation broadening by the blue laser intensity can be ruled out for three reasons. First, only about 10% of the atoms are actually excited into Rydberg states (roughly 60 000 atoms in the interaction volume are available in the $5P_{3/2}$ intermediate state) which can only explain a much smaller broadening than observed. Second, the line is asymmetrically broadened (see the inset of figure 6), and third, extensive density-dependent studies show that only the combination of high laser power with high densities results in the observed broadening [9]. We estimate an ionization rate due to collisions and black-body radiation of the order of 3 kHz [1] and therefore do not expect an appreciable number of ions to accumulate during the time of excitation ($\sim 20\,\mu$s). Electric fields due to ions in the vicinity of the Rydberg atoms can therefore not account for the observed broadening.

An intuitive picture for explaining the observed lineshapes is given in [21]. Line broadening is caused by off-resonant excitation of atomic pairs into a two-body interacting state with the energy shift being either due to long-range dipole–dipole forces or van der Waals interaction. The observed broadening thus directly reflects the interaction energy between pairs of Rydberg atoms. Note that under the conditions of our experiment, the interatomic spacing is still one order of magnitude larger than the extension of the electron wavefunction (nearest-neighbour distances are of the order of 5 μm compared to the $\sim 80^2 a_{\mathrm{Bohr}} \simeq 0.3\,\mu$m extension of the wavefunction). Following this interpretation, it is tempting to attribute the pronounced structure on the red wing of the resonances to the excitation of bound states in the attractive interatomic Rydberg–Rydberg potential [5]. Full resolution of these structures has so far been precluded by slow drifts of the blue excitation laser. As these structures seem to be very narrow we are currently setting up a stabilization scheme for the excitation laser, by locking it to a stable reference cavity in order to achieve the required stability in laser frequency.

Another interesting aspect apart from the line broadening is the effect of excitation suppression at the point of exact resonance. On resonance, atoms are excited and accumulated in the excited state. As more and more atoms are excited, the atomic transition shifts out of resonance due to interaction and the on-resonance excitation is suppressed. This effect has recently been studied by Tong *et al* [8] as a function of laser intensity and density for pulsed laser excitation, and by our group [9] as a function of density for cw excitation. In addition, our experiment allows for the study of excitation suppression as a function of cw excitation duration. The observations of Tong *et al* are nicely reproduced by a model which explicitly includes the interatomic van der Waals interactions [8]. Power saturation as the cause for the suppression of excitation probability with increasing intensity is carefully ruled out in these experiments. The on-resonance Rydberg excitation in figure 6 also saturates as a function of excitation intensity. However, in contrast to [8] a significant portion of atoms in the excitation volume is excited into Rydberg states. Therefore, saturation of the number of Rydberg atoms stems from both depletion of atoms in the launch state and an interaction-induced excitation blockade. The two effects cannot be disentangled easily from the data presented here.

In addition to the intensity dependence, we studied the number of Rydberg atoms as a function of the time for which the excitation laser is switched on, to gain more insight into the dynamics of the Rydberg excitation process in the regime of Rydberg–Rydberg interactions. The resulting spectra are shown in figure 7(a) with the 82S resonance appearing as the prominent line at $\Delta\nu = 0$ GHz. While the total width of the line increases with increasing excitation time, one observes an asymmetry in the line already at short excitation duration times, which supports the interpretation in terms of two-photon two-atom resonances. For a more quantitative analysis, however, a detailed model for the lineshape on the basis of predicted interaction potentials is needed. For long durations of excitation an additional feature appears at $\Delta\nu \approx -0.2$ GHz whose origin has not yet been clarified. The dipole-forbidden transition to 79ℓ states with $\ell \geqslant 3$ (broad feature centred around $\Delta\nu \simeq 1.5$ GHz) are excited due to the small residual electric fields mentioned above and become more prominent with increasing excitation time. Figures 7(b) and (c) show the peak height of the 82S and the 79ℓ line, respectively, as a function of excitation time.

As seen from figure 7(b), the number of atoms in the 82S state saturates with increasing excitation time. In order to describe the saturation of Rydberg excitation through depletion of launch state atoms we model the excitation process in the following way: the level structure of the atoms is reduced to an effective three-level system ($|g\rangle$, $|r\rangle$, $|d\rangle$) with the intermediate $5P_{3/2}$ state $|g\rangle$ coupled to the Rydberg state $|r\rangle$ which slowly decays into a state $|d\rangle$. The corresponding populations are N_g, N_r and N_d. The excitation rate into the Rydberg state is

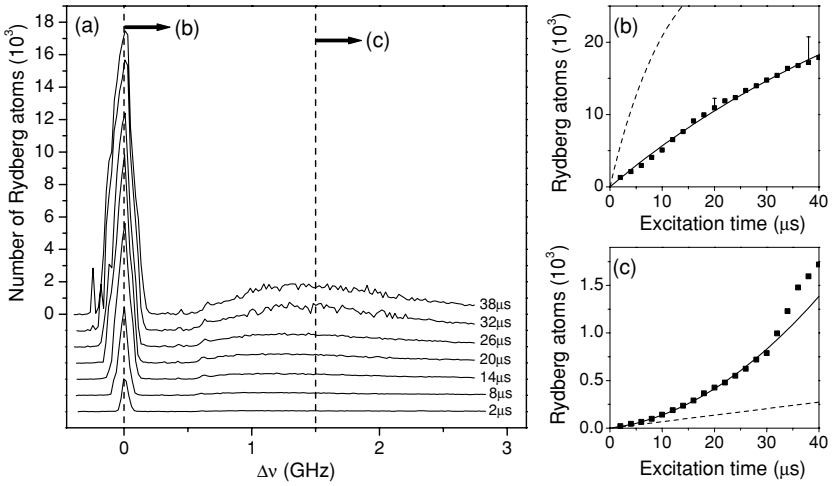

Figure 7. (a) Excitation spectrum of 82S and 79ℓ ($\ell \geqslant 3$) for different durations of the second excitation step driven by the blue laser. The graphs are offset for clarity with the duration time indicated on the right of each spectrum. The dashed lines indicate the frequencies of the atom number measurements depicted in (b) and (c). (b) Peak atom number for 82S as a function of excitation time. The curves show theoretic curves including induced and spontaneous emission. The solid line uses a fitted excitation rate, the dashed line uses an excitation rate extrapolated from low-power measurements. The error bars indicate the possible systematic errors due to MCP saturation mentioned in section 2.4. (c) Peak atom number for 79ℓ as a function of excitation time. The solid line shows a fit of a linear plus quadratic function. The dashed line depicts the linear term.

given by $R_{gr}N_g$ while stimulated emission occurs at a rate $R_{rg}N_r$, with the single atom coupling rate $R_{rg} = R_{gr} = R$ being proportional to the laser intensity. Spontaneous emission from $|r\rangle$ occurs mainly to states energetically close to $|r\rangle$ (see [1]) which are altogether represented by $|d\rangle$. Decay of $|d\rangle$ to $|g\rangle$ happens on a much slower timescale and is neglected here. We assume the first excitation step on the closed transition $5S_{1/2}(F = 2) \rightarrow 5P_{3/2}(F = 3)$ to be saturated. Then the dynamics of this system is described by the set of equations

$$N_g = \tfrac{1}{2}(N_{\text{total}} - N_r - N_d) \qquad \dot{N}_r = +RN_g - RN_r - \gamma N_r \qquad \dot{N}_d = +\gamma N_r \tag{1}$$

with $N_r(t = 0) = N_d(t = 0) = 0$ and γ representing the decay rate of the 82S state. Its value is taken from the literature as $\gamma = 1/560\,\mu\text{s} + 1/290\,\mu\text{s} = 1/191\,\mu\text{s}$, the two terms in the sum representing spontaneous decay and black-body-induced decay, respectively [1]. $|g\rangle$, corresponding to $5P_{3/2}$, is assumed to be permanently refilled from $5S_{1/2}$ to 50% of the number of atoms not being in states $|r\rangle$ or $|d\rangle$. $N_{\text{total}} \simeq 10^5$ is the total number of atoms in the excitation volume. The only free parameter is the Rydberg excitation rate R. The solid line in figure 7(b) shows a fit to the data. For comparison, the dotted line in figure 7(b) shows the solution of the above differential equations using the excitation rate which we extrapolated from measurements at low laser intensity.[3] The discrepancy between the low-power extrapolation and the model fit to the data may indicate that additional processes have to be included to describe the saturation of the Rydberg excitation. Indeed we believe this to be another, albeit weak sign for Rydberg–Rydberg interactions resulting in an inhibition of Rydberg excitation.

[3] From these low-power measurements (excitation rate 550 Hz, laser intensity 6 W cm^{-2}, specified laser-bandwidth 2 MHz) we extract the transition matrix element $\mu_{gr} = \langle 5P_{3/2}|ez|82S_{1/2}\rangle$ to be 3.4×10^{-4} au.

Another interaction-induced effect is seen in figure 7(c). It shows the excitation probability of the normally dipole-forbidden transition to the hydrogen-like 79ℓ ($\ell \geqslant 3$) states as a function of excitation time (measured as the Rydberg atom number at a detuning of +1.5 GHz with respect to the 82S line). If no interactions were present, this dipole-forbidden line should increase linearly with excitation duration. As shown in figure 7(c), the line centre grows much faster than linear. The data points up to 30 μs are fitted by a linear plus quadratic curve, the linear part being indicated by the dashed line. We attribute the quadratic growth of the Rydberg excitation to an increasing admixture of dipole-allowed states into the atomic states due to the interaction between the Rydberg atoms. In this way the excitation rate increases with growing number of Rydberg atoms, while the excitations due to the residual field act as a seed for this process.The strong increase of excitation for times longer than 30 μs has not yet been clarified and may be an experimental artefact. Further experiments including state-selective detection of the Rydberg atoms are needed to clarify the origin of the quadratic growth of dipole-forbidden lines in the presence of a small electric field. We are currently developing a model for the dipole interaction of Rydberg atoms in the presence of electric fields which may help us to gain insight into the dynamics of an interacting Rydberg gas.

5. Conclusion

In this paper we have described a compact experimental setup for the study of frozen Rydberg gases which combines state-of-the-art laser cooling and trapping techniques with two-photon cw excitation of high-lying Rydberg states. By qualitatively analysing the dependence of the excitation spectra on the intensity and the duration of the second excitation step we find indications for long-range interactions between Rydberg atoms. These findings are supported by more direct signatures for Rydberg–Rydberg interactions recently performed on the same experiment by studying the density dependence of resonance lines [9] and by investigating the intensity dependence of Rydberg excitation rates performed at the University of Connecticut [8].

At the largest Rydberg atom densities accessible to our experiment ($\sim 10^9$ Rydberg atoms per cm^3) we find spectroscopic features at the red-detuned side of the resonances which require further experimental investigations. The lineshapes and dependences of excitation rates on the different parameters are not yet quantitatively understood and require an appropriate model for the lineshapes based on the actual interaction potentials. Due to the rather long cw excitation times applied in our experiments, the model possibly has to include mechanical effects induced by the long-range interatomic Rydberg interactions. Progress in the quantitative description of these forces has recently been made [5, 22]. We hope that our experimental data will stimulate further theoretical investigations on the dynamics of interacting cold Rydberg gases.

Acknowledgments

We acknowledge financial support by the ‘Quantum Information Processing’ programme of the Landesstiftung Baden-Württemberg. We are grateful to D Schwalm for the generous support at the Max-Planck-Institute for Nuclear Physics in Heidelberg where these experiments were started. We thank A Mosk for his contribution in designing the experiment. Finally, we acknowledge many stimulating discussions and suggestions by P Gould, R Côté, E Eyler and L G Marcassa.

References

[1] Gallagher T F 1994 *Rydberg Atoms* (Cambridge: Cambridge University Press)
[2] Anderson W R, Veale J R and Gallagher T F 1998 *Phys. Rev. Lett.* **80** 249
[3] Mourachko I, Comparat D, de Tomasi F, Fioretti A, Nosbaum P, Akulin V M and Pillet P 1998 *Phys. Rev. Lett.* **80** 253
[4] Greene C H, Dickinson A S and Sadeghpour H R 2000 *Phys. Rev. Lett.* **85** 2458
[5] Boisseau C, Simbotin I and Côté R 2002 *Phys. Rev. Lett.* **88** 133004
[6] De Oliveira A L, Mancini M W, Bagnato V S and Marcassa G L 2003 *Phys. Rev. Lett.* **90** 143002
[7] Farooqi S *et al* 2003 *Phys. Rev. Lett.* **91** 183002
[8] Tong D, Farooqi S M, Stanojevic J, Krishnan S, Zhang Y P, Côté R, Eyler E E and Gould P L 2004 *Phys. Rev. Lett.* **93** 063001
[9] Singer K, Reetz-Lamour M, Amthor T, Marcassa L G and Weidemüller M 2004 *Phys. Rev. Lett.* **93** 163001
[10] Jaksch D, Cirac J I, Zoller P, Rolston S L, Côté R and Lukin M D 2000 *Phys. Rev. Lett.* **85** 2208
[11] Lukin M D, Fleischhauer M, Côté R, Duan L M, Jaksch D, Cirac J I and Zoller P 2001 *Phys. Rev. Lett.* **87** 037901
[12] Raab E L, Prentiss M, Cable A, Chu S and Pritchard D E 1987 *Phys. Rev. Lett.* **59** 2631
[13] Singer K, Tscherneck M, Eichhorn M, Reetz-Lamour M, Fölling S and Weidemüller M 2003 *Opt. Commun.* **218** 371
Singer K *et al* 2004 *German Patent* DE10243367A1
[14] Corwin K L, Lu Z -T, Hand C F, Epstein R J and Wieman C E 1998 *Appl. Opt.* **37** 3295
[15] Bjorklund G C 1980 *Opt. Lett.* **5** 15
[16] Singer K, Jochim S, Mudrich M, Mosk A and Weidemüller M 2002 *Rev. Sci. Instrum.* **73** 4402
[17] Lett P D, Watts R N, Westbrook C I, Phillips W D, Gould P L and Metcalf H J 1988 *Rev. Sci. Instrum.* **61** 169
[18] Fölling S 2003 *Diploma Thesis* University of Heidelberg
Singer K 2004 *PhD Thesis* University of Freiburg
[19] Luc-Koenig E, Liberman S and Pinard J 1979 *Phys. Rev.* A **20** 519
[20] Zimmerman M L, Littman M G, Kash M M and Kleppner D 1979 *Phys. Rev.* A **20** 2251
[21] Raimond J M, Vitrant G and Haroche S 1981 *J. Phys. B: At. Mol. Phys.* **14** L655
[22] Singer K, Stanojevic J, Weidemüller M and Côté R 2005 *J. Phys. B: At. Mol. Opt. Phys.* **38** S295